A Nucleic Acid Switch Triggered by the HIV-1 Nucleocapsid Protein†

Christopher L. DeCiantis,‡ Danielle K. Jensen,‡,§ Bruce S. Hudson,‡,|| and Philip N. Borer*,‡,||

Department of Chemistry, Syracuse University, Syracuse, New York 13244, and OrthoSystems, Inc., 111 College Place, 2-212 CST, Syracuse, New York 13244

Received January 7, 2007; Revised Manuscript Received May 15, 2007

ABSTRACT: A unimolecular oligonucleotide switch, termed here an AlloSwitch, binds the mature HIV-1 nucleocapsid protein, NCp7. This switch can be used as an indicator for the presence of free NCp7 and NC domains in precursor and fusion proteins. It is thermodynamically stable in two conformations, H and O. A FRET pair is covalently attached to the strands to report on the molecular state of the switch. The results show that NC has an affinity for O 170 times higher than its affinity for H and that in the absence of NC the equilibrium ratio $K_1 = [O]/[H] = 0.10 \pm 0.03$ for the switch sequence reported here. The change between the two states happens on a rapid kinetic time scale. A framework is introduced to aid in the design of AlloSwitches aimed at other targets. A high-affinity probe segment must be available to bind the target in the O-form, while a cover segment hides the probe in H. A key is adjusting the cover sequence to favor the H-form by a factor of 10−1000. This affords a robust response to small changes in target concentration, while saturation produces more than 90% of the maximal change in fluorescence. When a competitor displaces the switch from the NC−O complex, the released switch reverts to the H-form. This is the basis for a mix-and-read strategy for high-throughput screening of anti-nucleocapsid drug candidates that is much simpler to execute than traditional assays that require immobilization and washing steps.

The global HIV/AIDS epidemic continues to cause widespread suffering and death. The most widely used anti-retroviral agents fall into two categories: protease (PR) and reverse transcriptase (RT) inhibitors, nearly all of which have resistant strains (*1*). To continue the long-term treatment of the HIV-infected population, new anti-retrovirals will be required. While the search continues for new anti-PR and anti-RT agents, targeting other critical pathways in the viral infection cycle is a high priority (*2*−*9*). The HIV-1 nucleocapsid protein (NC) is involved in several processes in the viral replication cycle, including the packaging of the viral genome into budding virus particles (*10*−*15*). This makes it an attractive target for future anti-retroviral therapies (*16*−*19*). The binding affinity of NC for the HIV-1 5′-leader sequence has been studied extensively (*12*, *13*, *20*−25), including the determination of the binding affinities of the four stem−loop sequences (SL1−SL4) in this region for the mature 7 kDa nucleocapsid protein, NCp7[1] (*21*−23).

The most important determinant of packaging is stem−loop 3 (SL3). SL3 is sometimes termed the Ψ-loop or packaging loop, as its removal reduces packaging efficiency by ∼90% (*10*). However, interactions probably occur at several sites to provide full packaging specificity (*10*−*13*, *20*, *26*−*28*). An atomic-level structure of the SL3−NCp7 complex shows that the key interactions involve the second and fourth (G) residues in the GGAG tetraloop (*14*). We have examined more than a thousand sequences in GenBank containing SL3 and find that these two residues do not vary more than the rate of sequencing errors (*29*). Thus, targeting the NC−SL3 interaction for drug interdiction may hold special promise with respect to the inability of the virus to escape anti-NC drugs by mutation.

NC has both specific and nonspecific modes of interaction with genomic RNA (*30*). The nonspecific NC−RNA interaction dominates in the mature virion where there is roughly one NCp7 per 10 nucleotides. This causes the RNA to condense to a chromatin-like consistency. A RNA segment is expected to be bound by the protein if it has a K_d of <1 mM for NCp7 at the concentrations of the components in the mature nucleocapsid. Electrostatic interactions also play an important role because of the high formal charges involved, +9 for Zn_2·NCp7 and −15 to −20 for most of the RNA constructs we have examined (*21*−*23*, *31*). The nonspecific binding mode has a high affinity at low salt concentrations but can be suppressed by working at ionic strengths of ≥0.2 M (*31*); this is near-physiological conditions in blood where the ionic strength is ∼0.18 M, ignoring contributions of charged macromolecules (*32*). In 0.200 M NaCl (ionic strength of 0.206 M in NCp7 binding buffer, vide infra), wild-type SL3-GGAG has a K_d of 28 nM for NCp7 (*21*), while the variant, SL3-GGUG, binds even more tightly [$K_d = 10$ nM (*22*)]. NC has an affinity for base-paired

† Supported in part by NIH Grants R42 GM68413 and R01 GM32691.

* To whom correspondence should be addressed. E-mail: pnborer@syr.edu.

‡ Syracuse University.

§ Present address: Harvard Medical School, 200 Longwood Ave., WAB 260, Boston, MA 02115.

|| OrthoSystems, Inc.

[1] Abbreviations: SL3, stem−loop 3 with unpaired residues at G317-G318-A319-G320 of the 5′-leader of HIV-1 genomic RNA; NCp7, HIV-1 nucleocapsid protein; K_d, equilibrium constant for the dissociation of a bimolecular complex; FAM, 6-hydroxyfluorescein; P_t, total concentration of protein; S_t, total strand concentration of switch; FRET, fluorescence resonance energy transfer.

10.1021/bi700031j CCC: $37.00
Published on Web 07/21/2007

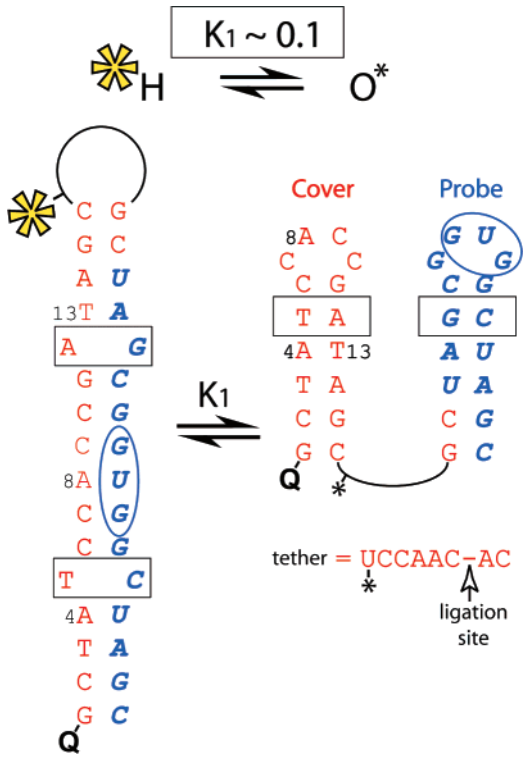

FIGURE 1: H-Form of the NC AlloSwitch (C3) (left) and its O-form (right). DNA is colored red and RNA blue (bold italics); the high-affinity GUG sequence is in the blue oval. A DNA tether sequence is shown as a black arc; its sequence is shown at the bottom right. The asterisk is a fluorophore, and Q is a fluorescence quencher. A large asterisk denotes the more highly fluorescent species.

sequences ~1000 times lower than its affinity for SL3-GUG (*22*), and a very low affinity for unpaired C and A bases (*22*, *33*, *34*).

Our characterization of the high-affinity interactions with the RNA loops in the packaging domain led us to construct a unimolecular oligonucleotide switch that is in equilibrium between two different base-paired conformations (Figure 1). In the results reported here, one form has the SL3-GUG sequence open (O) to bind NC; in the other form, the tetraloop bases are hidden (H) in a base-paired region. The equilibrium shifts from H to O upon addition of NC. The attachment of a fluorophore and quencher to the chain causes the fluorescence properties to differ for the two forms of the switch. We determine the equilibrium constant that relates the H- and O-forms and describe methods to set this equilibrium to favor H by a factor of 10−1000; this makes a switch that responds to relatively small changes in NC concentration.

The allosteric response of the nucleic acid upon ligand binding suggests the term AlloSwitch[2] for this class of bistable nucleic acid structures [the term "riboswitch" is now fairly common (*35*−*38*), but our molecules contain both DNA and RNA and could contain non-nucleic acid constituents, as well]. The idea of switchable conformations does not originate with us. Nature uses allosteric control to switch the state of enzymes and many other biological systems. Changes in nucleic acid structure regulate many cellular processes, e.g., gene expression (*35*−*38*), dimerization of HIV-1 RNA (*39*−*43*), Holliday junctions (*44*, *45*), ribozymes (*46*−*48*), and others (*49*−*51*), among thousands of nucleic acid-related switches. Other workers have also used RNA−DNA conformational switching to produce interesting structures or reporter systems for analytical purposes (*52*−*59*).

Designing the RNA−DNA chimera as a unimolecular system allows for intrinsic advantages over bimolecular arrangements such as those discussed in refs *52*−*58*. A unimolecular switch is easily reversible and can be used over any concentration range where the reporter signal is above the lower limits of detection. A bimolecular switch is limited by the concentrations of the two associating strands and is not readily reversible if dissociation occurs at low strand concentrations. A reversible system is well-suited to high-throughput screening of small molecules that can interrupt a protein−nucleic acid interaction.

The chimeric arrangement preserves the higher affinity of NC for RNA over DNA loops (*22*, *31*), while using DNA for the cover and tether sequences reduces the contribution of NC binding at these segments required for conformational switching. It also confers extra nuclease resistance and reduces the cost of labeling with fluorophore and quencher. The Discussion includes guidelines for designing AlloSwitches with appropriate [H]/[O] ratios. These guidelines apply for AlloSwitches consisting of all DNA, all RNA, or modified nucleic acids as long as appropriate thermodynamic data are available to predict relative free energies of the H- and O-forms.

Any naturally occurring or experimentally selected oligonucleotide−protein interaction with a known and stable structure could be developed into an AlloSwitch. These switches may be useful as real-time diagnostic indicators for contaminants or toxins. They can also be used as mix-and-read indicators in high-throughput searches for drug leads. They can have binding affinities for their targets similar to those of antibodies but do not require immobilization or washing steps (C. L. DeCiantis, M. McPike, S. Athavale, L. Chen, M. Shubsda, B. S. Hudson, and P. N. Borer, manuscript in preparation).

EXPERIMENTAL PROCEDURES

Oligonucleotides. The full-length DNA−RNA chimeric AlloSwitch, C3a, 5′-dabsyl-d[GCTATCCACCGATAGC(5-N-U)CCAACACGC]UAGCGGUGGCUAGC-3′ (Figure 1), was synthesized and gel purified by Dharmacon (Lafayette, CO) where d(5-N-U) was postsynthetically modified to covalently attach 6-carboxyfluorescein (FAM) via a six-carbon linker at the 5-position of dU, and a dabsyl at the 5′-end. The 2′-protecting groups were then removed from the RNA as instructed by the manufacturer. The sample was evaporated to dryness on a SpeedVac and resuspended in nuclease free water at a concentration of ~400 μM. The purity of the oligonucleotide was checked on a denaturing gel (12% PAGE, SequaGel, National Diagnostics) and did not require further purification. Unlabeled chimeras C1, C2, and C3 (sequences in Figure 1 and Table 1) and RNA constructs for SL2 and SL3 (sequences in refs *21*, *22*, and *31*) were also obtained from Dharmacon. These were HPLC purified on a Dionex 4 mm × 250 mm DNApac PA100 column using a 0.0050 to 0.150 M sodium perchlorate gradient in 0.010 M Tris and 2% acetonitrile (pH 8), followed by 2′-deprotection and desalting with a Waters Corp. C18

[2] AlloSwitch is a trademark of OrthoSystems, Inc.

Table 1: Mismatch Positions and Predicted K_1 Values for Three Switch Constructs[a]

	C1 ($K_1 = 6 \times 10^{-9}$)	C2 ($K_1 = 4 \times 10^{3}$)	C3 ($K_1 = 0.08$)
position 3	T	A	
position 4	A	T	
position 5	G		T
position 8	A	T	
position 9	C		
position 12	C		A
position 13	T	A	
position 14	A	T	

[a] Position shows the variable part of the cover sequence, listing all entries for the fully paired chimera, C1. Blank entries for C2 and C3 signify that the site has the same base as in C1. Refer to Figure 1 for the sequence positions.

Sep Pak cartridge by the Dharmacon protocol. Prior to use in titrations or assays, oligonucleotides were denatured by heating at 90 °C for 2 min and then cooled to 1 °C. Extinction coefficients for the oligonucleotide sequences were estimated at $N \times 8000$ cm^{-1} M^{-1} at 260 nm, where N is the chain length (*21*, *22*, *60*, *61*).

Ligation. C3bL, a 22mer DNA molecule with the sequence 5′-FAM-d[GCTATCCACCGATAGC(5-methyl red-U)CCA-AC-OH], was purchased as a HPLC-purified oligonucleotide from Eurogentec (Herstal, Belgium) and required no further purification. C3bL encompasses the cover strand and ends at the ligation site in Figure 1. C3R, encompassing the probe sequence at the right of Figure 1, was purchased from Dharmacon [5′-p-d(ACGC)UAGCGGUGGCUAGC-OH]. It has a 5′-phosphate followed by four DNA residues, and then 14 RNA residues. The molecule was purified by Dionex HPLC as described above. The 17mer DNA splint strand, d(CACCGCTAGCGTGTTGG), was purchased from Integrated DNA Technologies (Coralville, IA) and HPLC purified.

Ligation reaction mixtures included all oligonucleotide components at 5 μM (C3bL, C3R, and splint). The solution of oligonucleotides in water was heat cycled on a heating block to 85 °C for 2−3 min, gently vortexed to mix, briefly centrifuged, and cooled to room temperature for 10 min and then placed on ice for 5 min. 10× Ligase Buffer (New England Biolabs, Inc.) was added, followed by T4 DNA ligase (1 μL of enzyme/20 μL of reaction mixture). The mixture was incubated at 16 °C in the dark, with fresh additions of ligase at 10−20 h intervals. The progress of ligation was followed using 12% PAGE gels with samples loaded in a 1/1 mixture with a 1/1 solution of formamide and 7.5 M urea. Bands corresponding to C3bL and the full-length C3b AlloSwitch could be visualized under UV illumination at 365 nm. Analytical gels were then stained with StainsAll (Sigma) to locate both fluorescent and nonfluorescent strands. When the ligation was essentially complete, the reaction was quenched by heat inactivation of the ligase at 60 °C for 30 min, and the mixture was stored at −20 °C until needed for further experiments.

The preparative ligation reaction (300 μL) was quenched and the mixture concentrated using a Centricon YM3 apparatus (Millipore) to 70 μL. This was run on a denaturing PAGE gel. The bands were visualized under UV illumination at 365 nm, and the band corresponding to the C3b switch was excised with a clean razor blade, electroeluted, desalted, and concentrated.

NCp7 Preparation. The 55-amino acid NCp7 protein was prepared as described previously (*62*). The NCp7 concentration was determined by UV in the storage buffer [0.050 M Tris (pH 8.0), 10% glycerol, 0.10 M NaCl, 0.0001 M $ZnCl_2$, and 0.010 M β-mercaptoethanol], using an extinction coefficient at 280 nm of 6050 cm^{-1} M^{-1} (*21*, *22*). Aliquots at 50−200 μM in storage buffer were flash-frozen and stored at −80 °C.

NCp7 Trp Binding Assays. NCp7 binding buffer [0.0050 M sodium phosphate, 0.200 M sodium chloride, 0.0001 M zinc chloride, and 0.0025% PEG 8000 (pH 7.0)] was prepared as either a 1× or 5× stock and filtered through a 0.22 μm filter before being used in the assays. The initial W37 fluorescence at 350 nm of 0.3 μM NCp7 in 2.0 mL of buffer in a 10 mm × 10 mm quartz fluorescence cuvette was obtained using a QuantaMaster-4/2005 sensitivity-enhanced (QM-4/2005 SE, Photon Technology International) fluorescence spectrophotometer using a 290 nm excitation wavelength, a 4 nm excitation bandpass, and a 1.5 nm emission bandpass. An 8 mm × 1.5 mm Teflon-coated stir bar was also placed in the cuvette for mixing; the stir bar does not interfere with the light path in the cuvette. The assay mixture is continually stirred while it is in the fluorometer. Oligonucleotide was titrated into the cuvette in 2−4 μL increments from a 50 μM stock solution. The fluorescence was measured after addition of each aliquot of oligonucleotide. The fluorescence titration curve was fit to a model assuming a 1/1 stoichiometry to determine a K_d value (*21*). Each oligonucleotide was heat cycled prior to analysis.

C3a AlloSwitch Binding Assay. Individual wells of a 96-well, nontreated, medium-binding, flat-bottom, black plate (Greiner 655076) were filled with 150 μL of NCp7 binding buffer, a final concentration of 40 nM C3a AlloSwitch, and a final concentration of 0−12 μM NCp7. After the contents were mixed by pipetting, the fluorescence of the plate was read by exciting it at 485 nm and detecting the emission at 538 nm with an emission cutoff of 515 nm using a plate reader (Molecular Dynamics, SpectraMax Gemini).

Response of C3b AlloSwitch to NCp7 and Hydrolysis. A 2.0 mL aliquot of an ∼10 nM solution of C3b AlloSwitch in NCp7 binding buffer was placed in a cuvette equipped for mixing, as described above. The initial fluorescence at 517 nm was measured using the QM-4/2005 fluorometer using a 492 nm excitation wavelength, a 4 nm excitation bandpass, and a 1.5 nm emission bandpass. NCp7 was added to the cuvette to a concentration of ∼5 μM protein, which produces near saturation of the switch with protein. Several units each of RNase I (Promega) and RNase A (Sigma) were subsequently added to the sample of C3a in addition to the NCp7 that had already been added (above). The RNA was fully hydrolyzed within 20 min at room temperature, using the lack of any further decrease in fluorescence as the gauge of completion. To this solution was added 7 μL of a 1 unit/μL RQ1 DNase I solution (Promega), and the solution was held at room temperature in the dark. The fluorescence was measured several times over a 72 h period, after which no further change occurred. One unit of RNase I degrades RNA at a rate of 100 ng/s at 37 °C in 10 mM Tris-HCl (pH 7.5 at 25 °C), 5 mM EDTA, 200 mM sodium acetate, 0.2 μg/μL RNA, 0.05% NP-40, and 2 μg/μL BSA. One unit of RNase A produces an increase of 1.0 A_{260} unit/min when yeast RNA is hydrolyzed at 37 °C at pH 5.0. One unit of RQ1 RNase-

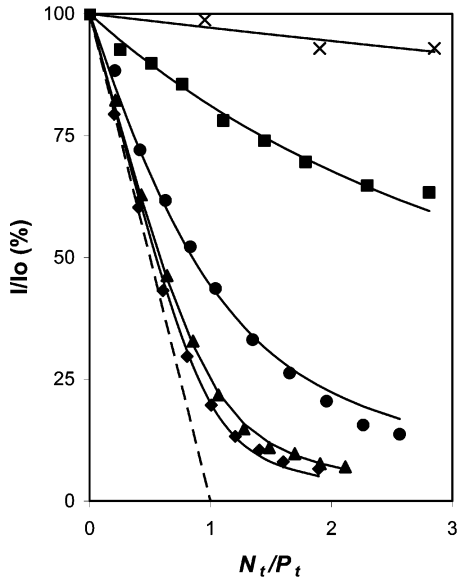

FIGURE 2: Tryptophan fluorescence titrations of NCp7 protein (P_t = 0.3 μM) with oligonucleotide (at strand concentration N_t). Data (from top to bottom) are as follows: DNA 16mer DNA cover hairpin (×; $K_d \cong 10$ μM), switch locked in H (■, molecule C1; $K_d \cong 1.0$ μM), active switch [●, C3; K_d(apparent) = 110 ± 20 nM], SL3 RNA (▲; K_d = 25 ± 2 nM), and switch locked in O (◆, C2; $K_d \cong 6$ nM). The best-fit values of K_d listed above were used to generate the solid lines. The dashed line is for a 1/1 complex with an infinite binding constant.

Free DNase completely degrades 1 μg of DNA in 10 min at 37 °C in 50 μL of a buffer containing 40 mM Tris-HCl (pH 7.9 at 25 °C), 10 mM NaCl, 6 mM $MgCl_2$, and 10 mM $CaCl_2$.

RESULTS

The sequence and secondary structure of a NC AlloSwitch are shown in Figure 1. The RNA GGUG tetraloop and SL3 stem is the "probe" sequence. Its critical GUG sequence is open and available to bind NC in the O-form of the switch at the right. This sequence is hidden in standard base pairs in the H-form at the left of Figure 1. The DNA "cover" sequence at the 5′-end was designed to make the H-state slightly more stable than the double-hairpin O-form. The cover and probe segments are covalently linked by a tether sequence, d[(U-*)CCAACAC], as shown in Figure 1, where dU-* has a fluorophore attached at the 5-position of deoxyuridylate.

Several cover strand sequences were designed to allow the equilibrium constant, K_1, for the H- and O-forms to vary over a wide range (see the Discussion). Table 1 shows three of these. C1 is designed to be locked in the H-form, which has four more base pairs than the O-form. C2 is designed to be locked in the O-form, introducing five mismatches in H while preserving all of the base pairs in O. C3 is designed to be an active switch with a K_1 of ~0.1.

Tryptophan Fluorescence Assay. The Trp assay data in Figure 2 were used to characterize functional and locked switches and their components. The cover DNA hairpin of the O-form (see Figure 1) binds very weakly to NCp7 ($K_d \cong 10$ μM), as does C1, designed to be locked in the H-form ($K_d \cong 1.0$ μM). The functional switch, C3, has a K_d(apparent) of 110 ± 20 nM. The molecule locked in the O-form, C2, has a K_d of ≅6 nM. Stock solutions of the protein can degrade, so a positive control titration with SL3 was performed daily; the curve shown in the figure has a K_d of 25 nM, very near the published value of 28 nM (*21*).

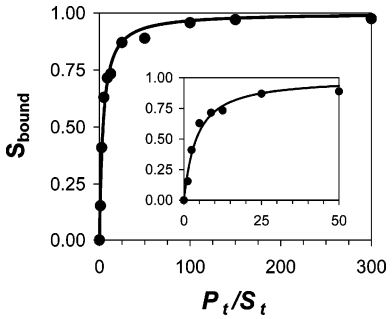

FIGURE 3: Fraction of bound C3a switch (S_t = 40 nM) as the total NCp7 concentration (P_t) increases. The inset details the first eight points in the series. Solid lines show the fit with a K_d(apparent) of 140 ± 20 nM.

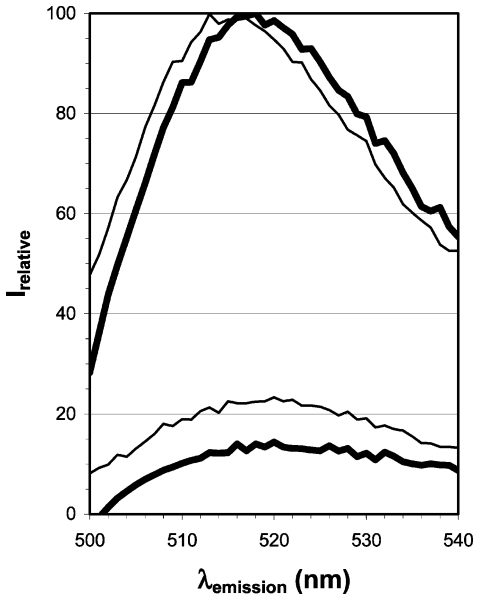

FIGURE 4: Thin lines are fluorescence emission spectra of free C3b switch (top) and upon addition of a nearly saturating amount of NCp7 (bottom). Heavy lines are spectra of the limit digest after addition of RNase (bottom) and the limit digest after addition of DNase (top).

Switch Signaling. NCp7 was added to the C3a switch in an assay using a 96-well microtiter plate and a fluorescence plate reader to quantify the response to additions of NCp7. Figure 3 shows the fraction of bound switch versus P_t/S_t, the mole ratio of total protein to total switch; S_t = 40 nM in each well. Data points are averages for 12 replicates for P_t/S_t = 0−50 (mean of 95% confidence limits = ±1.4%), eight replicates for ratios of 100 and 150 (±0.8%), and three for 300 (±4.0%). The best-fit K_d(apparent) = 140 ± 20 nM.

Addition of NCp7 to an ~10 nM solution in the C3b switch is illustrated in Figure 4. The thin curve at the top shows the fluorescence from the free switch. The other thin curve shows the result of the addition of a large excess of NCp7 (the amount of NCp7 produces >90% saturation of the switch). The minimum and maximum intensity spectra were estimated by addition of nucleases. When ribonuclease was added to the solution containing switch and the final aliquot of NCp7, the limit digest had the spectrum shown as the bottom (heavy) trace in Figure 4. Addition of DNase

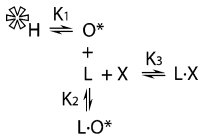

FIGURE 5: Equilibria relating the H- and O-forms of an AlloSwitch, a protein ligand, L, which binds the probe sequence in the O-form, and X, a molecule that competes with O for L.

led to the top (heavy) spectrum in the limit digest. (All fluorescence curves were normalized to the maximum intensity of this spectrum.)

DISCUSSION

The scheme in Figure 5 allows detailed analysis of an AlloSwitch-based system for signaling the presence of a binding ligand, L (L = NC in this paper). The K_1 equilibrium (K_1 = [O]/[H] ≅ 0.1) favors the "bright" H-form in the absence of the ligand. As L is added, it binds the probe to produce increasing amounts of the "dark" L·O complex via the K_2 equilibrium, which reduces the concentration of the free O-form. The K_1 equilibrium adjusts to produce more O so [H] approaches zero at a sufficiently high [L], and the fluorescence goes to a minimum. Thus, each well in a microtiter plate would have low fluorescence when the switch is nearly saturated with L.

Addition of the K_3 equilibrium offers an opportunity for high-throughput screening of anti-NC drug candidates. Interesting candidates that bind appreciably to L at concentration X_t will displace O, which reverts to the bright H-form via K_1. The set of three coupled equilibria can be used to define appropriate concentrations of L_t, S_t, and X_t, to distinguish interesting candidates by bright wells in the plate. This is a simple mix-and-measure assay that requires no immobilization, washing, or secondary readout common in many high-throughput screens. Given the sensitivity of FRET-based detection, the cost per well of the switches is likely to be far less than in antibody-based assays. As the lead candidates undergo refinement toward useful drugs, the same system can be used in low-throughput mode to assess K_d(K_3) values for the derivatives.

A key feature of the AlloSwitch system is that the sequence of the cover strand can be varied such that a relatively small change in [L] will produce a substantial change in fluorescence. This can be achieved by setting K_1 in the range from 0.1 to 0.001. With the arrangement of fluorophore and quencher in Figure 1, this gives an unbound switch that has 90−99.9% of the fluorescence of the pure H-form. Adding protein suppresses this signal, which can be easily restored by a potentially interesting drug candidate. This paper is primarily concerned with characterizing K_1 for the AlloSwitch in Figure 1.

Relative Affinities for NC Measured by Tryptophan Fluorescence. The single tryptophan in NCp7 becomes quenched when the protein binds nucleic acid (*21*, *22*, *24*, *63*−*66*). While controversy regarding the absolute affinities of NCp7 for stem−loop sequences from the HIV-1 leader RNA remains (*21*−*25*, *33*, *61*, *67*−*70*), the simple and highly sensitive Trp fluorescence assay determines the relative affinities of RNA and DNA sequences for NC (*21*−*23*, *31*). High-resolution structures suggest that efficient quenching is due to stacking of nucleobases on W37 (*14*, *24*, *65*). K_d values from Trp fluorescence quenching assays have been shown to be highly reproducible in 0.2 M NaCl and clearly distinguish the relative affinities of various RNA and DNA loops (*22*, *31*). The precision is typically ±10% (*21*−*23*, *31*) unless K_d < 10 nM (where such a low [NC] is required that sensitivity is reduced) or K_d > 1000 nM (where a very high nucleic acid concentration is required to approach saturation; this can lead to stoichiometries that have excess RNA or DNA). Both protein-excess and RNA/DNA-excess complexes have been identified (*21*, *25*, *31*, *71*). Early points in titrations as in Figure 2 favor protein-excess complexes as they have much more protein than nucleic acid on a molar basis. Experiments in our laboratory show that complexes with stoichiometries other than 1/1 cannot be present at more than ∼10% in Trp-monitored titrations at ≥0.2 M NaCl (S. Athavale et al., manuscript in preparation).

The Trp assay data in Figure 2 were used to characterize locked switches and their components. As expected, the cover DNA hairpin of the O-form (see Figure 1) binds very weakly to NCp7 (K_d ≅ 10 μM). This is an affinity 400 times lower than that for the positive control titration (SL3, K_d = 25 nM in Figure 2). C2 (K_d ≅ 6 nM), designed to be locked in the O-form, binds NC with an even higher affinity than the control. This value is similar to that for the single RNA stem−loop SL3-GUG [K_d = 10 ± 1 nM (data not shown and ref *22*)], which comprises the right half of the O-form switch in Figure 1. By contrast, C1 (K_d = 1.0 μM), designed to be locked in the H-form, binds NC with an affinity 170 times lower than that of C2, so there is no need to consider effects due to binding of NC to the H-form. The active switch, C3 [K_d(apparent) = 110 ± 20 nM], binds NC less tightly than C2 because the dominant H-form must be converted to the higher-free energy O-form to bind NC. None of these molecules carried an attached fluorophore or quencher. All of the binding isotherms in Figure 2 lie to the right of the dashed line as expected for a 1/1 stoichiometry; this is inconsistent with complexes having more than one protein bound per nucleic acid (*21*, *22*).

The Trp assay data in Figure 2 allow a reasonable estimate of K_1 for the active switch molecule, C3. The apparent dissociation constant [K_d(apparent)] providing the best fit to the C3 binding isotherm (●) equaled 110 ± 20 nM. The K_1 equilibrium affects the dissociation according to the relation K_d(apparent) = K_d(1 + 1/K_1), where K_d is the dissociation constant for dissociation of NC from the probe segment of C3 and K_1 = $[O]_{free}/[H]_{free}$. A K_1 value of 0.10 ± 0.03 is calculated by assuming that the dissociation of NC from the open probe segment is the same as that from SL3-GUG (K_d = 10 ± 1 nM).

Switch Signaling. A change in fluorescence occurs with the change in state from H to O by virtue of placing a quencher at the 5′-end of the chain (Q in Figure 1) and a fluorophore at the location marked with an asterisk (∗). In the C3a AlloSwitch, the signaling arrangement has ∗ = FAM and Q = dabsyl. In C3b, the positions of ∗ and Q are swapped and Q = methyl red; other arrangements of ∗ and Q are also useful. In both C3a and C3b, the distance between the fluorophore and quencher is larger in H than in O, so H should have a higher fluorescence intensity. This effect is seen in Figure 4 where adding NC to the C3b switch produces the expected fluorescence decrease. These fluorophore/quencher signaling pairs are well-known in "molecular

beacons" that increase their fluorescence when bound to various RNA−DNA sequences (*72*, *73*). Unimolecular AlloSwitches are similar to "scorpion" probes used in real-time PCR applications (*74*, 75).

Figure 3 shows analysis of the fluorescence decrease for C3a upon addition of NCp7 measured using a plate reader; the best-fit K_d(apparent) = 140 ± 20 nM. Using a K_d of 10 ± 1 nM for the probe, as with the Trp assay in Figure 2, yields a K_1 of 0.08 ± 0.02 from a K_d(apparent) of $K_d(1 + 1/K_1)$. This is in excellent agreement with that determined above from tryptophan titrations with unlabeled switch components. Thus, it is unlikely that the FAM and dabsyl labels exert substantial effects on the K_1 and K_2 equilibria.

Too little of the C3b switch was produced by ligation to accurately quantify its concentration and estimate K_d(apparent). RNase treatment leaves the DNA cover sequence with the fluorophore and quencher near each other [the red hairpin in the O-form (Figure 1)]. The minimum fluorescence in the limit digest is shown as the bottom (heavy) spectrum in Figure 4. Again, examination of Figure 1 shows that hydrolysis by DNase should release the fluorophore and quencher from the DNA chain. The top thick curve in Figure 4 shows that the original fluorescence intensity is essentially restored in the limit digest.

There are effects due to sequence context on the maximum and minimum fluorescence of molecular beacons, presumably due to stacking of the aromatic dyes on the nucleobases (*76*). Stacking and steric occlusion may differ in the H- and O-forms of the AlloSwitches, which could affect the ON/OFF contrast ratio in C3a and C3b. The RNase experiment suggests that the signaling arrangement in C3b with 6-hydroxyfluorescein (FAM) as the fluorescence donor and methyl red as the quencher (switch C3b) is not capable of full quenching. The ratio of the fluorescence of the free switch to the RNase-hydrolyzed switch is 7.8 at 517 nM. In switch C3a, the fluorescence change is even lower, with an ON/OFF contrast ratio of 1.7 between the H- and O-forms. This switch placed a dabsyl quencher at the 5′-end and FAM at position 17 (see Figure 1). Part of the reduced contrast may be due to context effects and possibly to the fact that methyl red is a better quencher than dabsyl for fluorescein (*77*). We also experienced batch-to-batch variation in the ON/OFF contrast ratios for C3a switches, typically ±10−20%. The switches run as a single band on a denaturing PAGE gel, but it is possible that the postsynthetic labeling steps are not quantitative. The ON/OFF contrast ratio would be reduced if less than the full amount of quencher were attached. Other signaling arrangements are currently under investigation in our laboratories to increase the ON/OFF ratio. Even so, the C3a arrangement is useful in most applications as the changes in fluorescence are reproducible within micropipetting errors (±3−5%) for a given batch of switches.

Adjusting K_1 To Modulate Switch Response. A wide range of K_1 values can be achieved by picking a specific probe sequence and altering the DNA cover sequence. The free energies of candidate secondary structures can be surveyed using RNA/DNA folding programs (*78*−*80*). Table 2 illustrates the method of first approximation using the C1, C2, and C3 sequences and the RNAstructure program of Mathews et al. (*78*, *80*, *81*) that also incorporates parameters for DNA folding (*82*, *83*). For the NC switch, the maximum deviation from the lowest free energy can be set at 30% and window size at 2 in RNAstructure.

Table 2: Predictions of K_1 for Three Switch Constructs[a]

		RNA	DNA
C1	H	−33.8	−20.3
	O	−18.4	−11.1
	$\Delta G°$	15.4	9.2
	K_1	1.4×10^{-11}	3.3×10^{-7}
C2	H	−16.6	−8.3
	O	−18.2	−11.8
	$\Delta G°$	−1.6	−3.5
	K_1	13	290
C3	H	−20.4	−12.1
	O	−16.4	−9.8
	$\Delta G°$	4.0	2.3
	K_1	1.5×10^{-3}	2.4×10^{-2}

[a] Rows labeled H and O contain free energies in kilocalories per mole at 37 °C calculated using RNAstructure, version 4.4. Rows labeled $\Delta G°$ contain values of $\Delta G°$(O-form) − $\Delta G°$(H-form).

The first row in Table 2 is generated using the C1 sequence and folding as RNA and then as DNA. The GGUG probe sequence is hidden in a strongly base paired stem. The energy estimate is the free energy of folding from the reference state: the unstacked single strands. To generate the O-form free energies in RNAstructure, use the "Force" menu to force a pair between bases 1 and 16 with a helix length of six. As both the H- and O-forms have the same reference state, the difference in the energy values gives the $\Delta G°$ for H → O. This gives an estimate for K_1 in the range of 10^{-7} to 10^{-11}, weighted strongly in favor of the H-form, which has four more base pairs than O.

The second group of energies and K_1 values in the table was generated with the C2 sequence. Now both folds are within 30% of the minimum free energy. The estimates for K_1 are ∼10−300; the five mismatches introduced in the H-form make it less stable than the O-form.

The final set of entries in the table is for the C3 sequence, where again both folds are within 30% of the lowest free energy. The estimates for K_1 are roughly 0.001−0.02, which should be sufficient for a functional switch. At this point, it is most useful if there are only two major classes of folds: the most stable one where the probe is hidden and the second where the probe is open. Minor variations on the two main folds that are close in free energy may be acceptable, but care should be taken to eliminate those that might offer alternative binding sites for the ligand. For NC, these would be single strands with multiple G, U, or T residues. Trial-and-error iteration through several alternative sequences is relatively simple.

Table 1 presents only coarse estimates of K_1 for each sequence, as an error of 1.4 kcal/mol leads to a 10-fold error in K_1. The uncertainties in the free energy parameters in the databases are on the order of 1 kcal/mol, so even under ideal circumstances, the folding programs can be used only to guide experiments to optimize switches. Further, the current implementations of mfold are not parametrized for RNA−DNA hybrid stems, and the penalties for internal loops with RNA and DNA on opposite sides and for hairpins involving mixed RNA−DNA stems will differ from those in the databases.

Using a DNA−RNA hybrid database (*84*) can improve the accuracy of the process at the expense of additional labor.

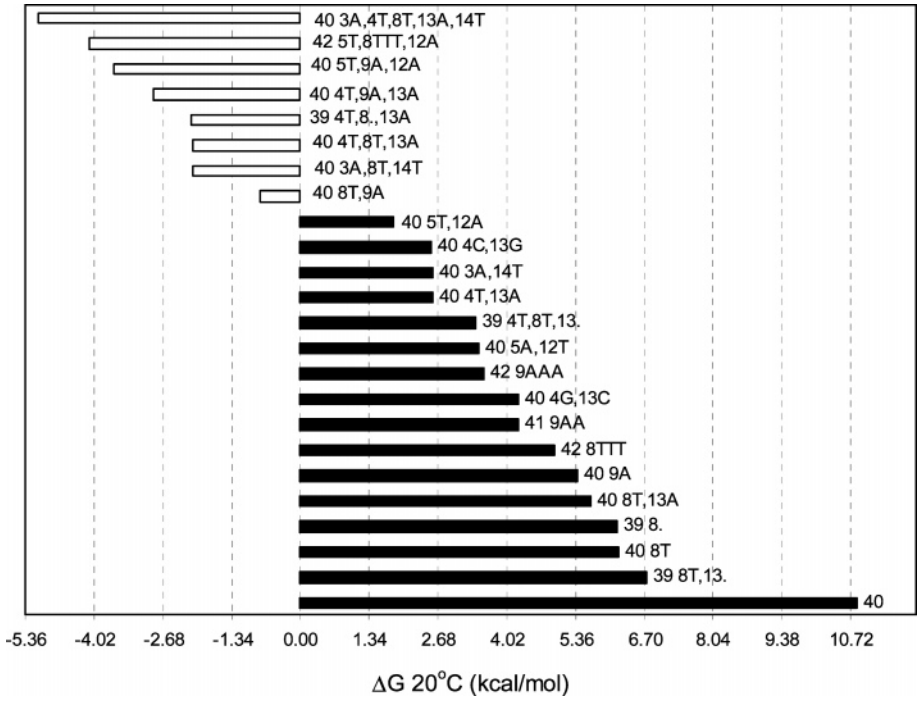

FIGURE 6: Calculated free energy differences [$\Delta G°$(O) − $\Delta G°$(H)] for some sequences of NC AlloSwitches. Sequences to the left (white bars) favor the O-form, while sequences to the right (black bars) favor the H-form. The vertical lines are spaced by 1 order of magnitude in K_1. The labels on each bar indicate the chain length and substitutions (capital letters) or deletions (periods) relative to sequence C1 in Table 1, which is the bottom bar labeled 40. The label for C2 from Table 1 is 40 3A,4T,8T,13A,14T, at the top. C3 is labeled 40 5T,12A, the top black bar.

Figure 6 shows a family of sequences and their calculated free energies, which can easily be converted to K_1 values. These calculations were guided by the procedures described by Serra and Turner (*85*), including their approximations for loop penalties. In addition, the enthalpies published in the databases were used to correct the $\Delta G°$ values for H → O conversion from 37 to 20 °C where our experiments were conducted. Sequences with a wide range of K_1 values are shown; this allows the creation of switches locked in the H- and O-forms, as well as candidates likely to have K_1 values in the desirable range between 0.001 and 0.1. When the calculations are applied to C3, the predicted $\Delta G°$(20 °C) = 1.80 kcal/mol, corresponding to a K_1 of 0.054, close to the estimates of 0.08−0.10 from titrations of C3 with NCp7. There is still enough uncertainty in the calculations that it will be rare to accurately predict K_1 within 1 order of magnitude. Thus, it will be important to experimentally determine the properties of a switch, its component stem−loop structures, and locked forms. The sequences in Figure 6 suggest bulge/internal loop modifications that may be useful for creating AlloSwitches for other targets. They also emphasize that rather fine-grained control should be possible over a range of 12 orders of magnitude in K_1.

Ligation versus Full-Length Synthesis. The choice of ligating half-molecules versus synthesis of the full-length molecule by solid-phase synthesis often comes down to relative cost and to which FRET dyes are conveniently attached in postsynthetic steps. For initial work, there may be a benefit in ligation as the thermodynamic predictions may not correctly forecast the K_1 value, and several unique half-molecules could be joined. Work in progress in our laboratories aims to develop experimental methods for simplifying the choice of which cover sequences work best with a specific probe.

Choice of FRET Pairs. Fluorescein as the fluorophore and dabsyl or methyl red as the quencher to signal the state of the AlloSwitch have an advantage in that they are commonly available in commercial postsynthetic labeling and are nonproprietary. Other FRET pairs may offer superior performance, although it is possible that certain dyes may alter K_1 if they interact differently with the switch stem−loop sequences from fluorescein and dabsyl. Particularly attractive for high-throughput screening of drug candidates are FRET pairs that transfer a blue region excitation toward a red emission. This moves the detection wavelength away from the blue/green portion of the spectrum where fluorescein emits and where many small molecule drug candidates also fluoresce.

The average distance from the fluorophore to the quencher in the H-form should be roughly 50 Å (see Figure 1; ∼16 bp in length × ∼3 Å per base pair in an A-form hybrid duplex), while the average in the O-form should be roughly the diameter of a B-form DNA duplex (∼25 Å). Thus, AlloSwitch applications could benefit from using dyes with Förster distances of >25 Å.

Chimeric AlloSwitches. The current design incorporates both RNA and DNA segments. The RNA binding probe was chosen due to the ∼10-fold increase in the affinity of the RNA GGUG loop over that of the corresponding DNA loop (*22*, *31*), while the DNA cover sequence was chosen for high-yield synthesis. An added bonus is the fact that the DNA segment provides some additional resistance to nucleases. It should be possible to make AlloSwitches that are all RNA or all DNA or incorporate any of the many modifications that are available via solid-phase nucleic acid synthesis. It should be simpler and more accurate to predict the relative free energies of the H- and O-forms for switches made from

all RNA or all DNA than for chimeric switches or those that incorporate modified backbones or bases.

Final Comments. The C3 AlloSwitch has characteristics that make it promising as an indicator for high-throughput screens of anti-NC drug candidates (C. L. DeCiantis, M. McPike, S. Athavale, L. Chen, M. Shubsda, B. S. Hudson, and P. N. Borer, manuscript in preparation). (i) The switch can be used in mix-and-read assays that do not require lengthy incubation or wash steps. (ii) The equilibrium fluorescence can be calibrated to measure the final concentration of NC in NCp7, GST-tagged NCp7, and gag-precursor proteins. (iii) It is easy to reverse the protein-induced change by adding SL2 RNA from HIV-1 [$K_d = 23$ nM (*21*)], which competes for the GUG binding site on the protein. (iv) The conformational change occurs within seconds of adding protein or competitor. (v) The NC AlloSwitch is highly selective; nontarget proteins such as glutathione *S*-transferase, lysozyme, and albumin have been incubated with the C3 switch and do not cause the conformational change. In addition, the strategies outlined here make it possible to create switches with RNA probes that respond to the presence of Tat, Rev, and other drug targets in HIV-1.

ACKNOWLEDGMENT

We gratefully acknowledge Dr. Mark McPike, Dr. Mike Shubsda, and Mr. Richard Yule for helpful discussions and Dana Schaefer for technical assistance. Ms. DeAnn Barnhart conducted some of the initial experiments on ligation of switch strands.

SUPPORTING INFORMATION AVAILABLE

A plot showing the average fluorescence of the C3a AlloSwitch upon addition of NCp7, together with 95% confidence limits. This material is available free of charge via the Internet at http://pubs.acs.org.

REFERENCES

1. Johnson, V. A., Brun-Vezinet, F., Clotet, B., Kuritzkes, D. R., Pillay, D., Schapiro, J. M., and Richman, D. D. (2006) Update of the drug resistance mutations in HIV-1: Fall 2006, *Top. HIV Med. 14*, 125−130.
2. Haffar, O., Dubrovsky, L., Lowe, R., Berro, R., Kashanchi, F., Godden, J., Vanpouille, C., Bajorath, J., and Bukrinsky, M. (2005) Oxadiazols: A new class of rationally designed anti-human immunodeficiency virus compounds targeting the nuclear localization signal of the viral matrix protein, *J. Virol. 79*, 13028−13036.
3. Westby, M., Nakayama, G. R., Butler, S. L., and Blair, W. S. (2005) Cell-based and biochemical screening approaches for the discovery of novel HIV-1 inhibitors, *Antiviral Res. 67*, 121−140.
4. Anthony, N. J. (2004) HIV-1 integrase: A target for new AIDS chemotherapeutics, *Curr. Top. Med. Chem. 4*, 979−990.
5. Bannwarth, S., and Gatignol, A. (2005) HIV-1 TAR RNA: The target of molecular interactions between the virus and its host, *Curr. HIV Res. 3*, 61−71.
6. Harrich, D., McMillan, N., Munoz, L., Apolloni, A., and Meredith, L. (2006) Will diverse Tat interactions lead to novel antiretroviral drug targets? *Curr. Drug Targets 7*, 1595−1606.
7. Yang, Q. E., Stephen, A. G., Adelsberger, J. W., Roberts, P. E., Zhu, W., Currens, M. J., Feng, Y., Crise, B. J., Gorelick, R. J., Rein, A. R., Fisher, R. J., Shoemaker, R. H., and Sei, S. (2005) Discovery of small-molecule human immunodeficiency virus type 1 entry inhibitors that target the gp120-binding domain of CD4, *J. Virol. 79*, 6122−6133.
8. Luedtke, N. W., and Tor, Y. (2003) Fluorescence-based methods for evaluating the RNA affinity and specificity of HIV-1 Rev-RRE inhibitors, *Biopolymers 70*, 103−119.
9. Li, F., and Wild, C. (2005) HIV-1 assembly and budding as targets for drug discovery, *Curr. Opin. Invest. Drugs 6*, 148−154.
10. Hayashi, T., Shioda, T., Iwakura, Y., and Shibuta, H. (1992) RNA packaging signal of human immunodeficiency virus type 1, *Virology 188*, 590−599.
11. Hayashi, T., Ueno, Y., and Okamoto, T. (1993) Elucidation of a conserved RNA stem-loop structure in the packaging signal of human immunodeficiency virus type 1, *FEBS Lett. 327*, 213−218.
12. Clever, J., Sassetti, C., and Parslow, T. G. (1995) RNA secondary structure and binding sites for gag gene products in the 5′ packaging signal of human immunodeficiency virus type 1, *J. Virol. 69*, 2101−2109.
13. McBride, M. S., and Panganiban, A. T. (1996) The human immunodeficiency virus type 1 encapsidation site is a multipartite RNA element composed of functional hairpin structures, *J. Virol. 70*, 2963−2973.
14. De Guzman, R. N., Wu, Z. R., Stalling, C. C., Pappalardo, L., Borer, P. N., and Summers, M. F. (1998) Structure of the HIV-1 nucleocapsid protein bound to the SL3 psi-RNA recognition element, *Science 279*, 384−388.
15. Harrison, G. P., and Lever, A. M. (1992) The human immunodeficiency virus type 1 packaging signal and major splice donor region have a conserved stable secondary structure, *J. Virol. 66*, 4144−4153.
16. Darlix, J. L., Cristofari, G., Rau, M., Pechoux, C., Berthoux, L., and Roques, B. (2000) Nucleocapsid protein of human immunodeficiency virus as a model protein with chaperoning functions and as a target for antiviral drugs, *Adv. Pharmacol. 48*, 345−372.
17. Musah, R. A. (2004) The HIV-1 nucleocapsid zinc finger protein as a target of antiretroviral therapy, *Curr. Top. Med. Chem. 4*, 1605−1622.
18. Schafer, A., Bogerd, H. P., and Cullen, B. R. (2004) Specific packaging of APOBEC3G into HIV-1 virions is mediated by the nucleocapsid domain of the gag polyprotein precursor, *Virology 328*, 163−168.
19. Cruceanu, M., Urbaneja, M. A., Hixson, C. V., Johnson, D. G., Datta, S. A., Fivash, M. J., Stephen, A. G., Fisher, R. J., Gorelick, R. J., Casas-Finet, J. R., Rein, A., Rouzina, I., and Williams, M. C. (2006) Nucleic acid binding and chaperone properties of HIV-1 Gag and nucleocapsid proteins, *Nucleic Acids Res. 34*, 593−605.
20. McBride, M. S., Schwartz, M. D., and Panganiban, A. T. (1997) Efficient encapsidation of human immunodeficiency virus type 1 vectors and further characterization of cis elements required for encapsidation, *J. Virol. 71*, 4544−4554.
21. Shubsda, M. F., Paoletti, A. C., Hudson, B. S., and Borer, P. N. (2002) Affinities of Packaging Domain Loops in HIV-1 RNA for the Nucleocapsid Protein, *Biochemistry 41*, 5276−5282.
22. Paoletti, A. C., Shubsda, M. F., Hudson, B. S., and Borer, P. N. (2002) Affinities of the Nucleocapsid Protein for Variants of SL3 RNA in HIV-1, *Biochemistry 41*, 15423−15428.
23. Yuan, Y., Kerwood, D. J., Paoletti, A. C., Shubsda, M. F., and Borer, P. N. (2003) Stem of SL1 RNA in HIV-1: Structure and Nucleocapsid Protein Binding for a 1 × 3 Internal Loop, *Biochemistry 42*, 5259−5269.
24. Amarasinghe, G. K., De Guzman, R. N., Turner, R. B., Chancellor, K. J., Wu, Z. R., and Summers, M. F. (2000) NMR structure of the HIV-1 nucleocapsid protein bound to stem-loop SL2 of the ψ-RNA packaging signal. Implications for genome recognition, *J. Mol. Biol. 301*, 491−511.
25. Hagan, N., and Fabris, D. (2003) Direct mass spectrometric determination of the stoichiometry and binding affinity of the complexes between nucleocapsid protein and RNA stem-loop hairpins of the HIV-1 ψ-recognition element *Biochemistry 42*, 10736−10745.
26. Coffin, J. M., Hughes, S. H., and Varmus, H. E. (1997) *Retroviruses*, Cold Spring Harbor Laboratory Press, Plainview, NY.
27. Clever, J. L., Eckstein, D. A., and Parslow, T. G. (1999) Genetic dissociation of the encapsidation and reverse transcription functions in the 5′ R region of human immunodeficiency virus type 1, *J. Virol. 73*, 101−109.
28. Clever, J. L., and Parslow, T. G. (1997) Mutant human immunodeficiency virus type 1 genomes with defects in RNA dimerization or encapsidation, *J. Virol. 71*, 3407−3414.
29. Lin, Y. (2002) Database and algorithmic applications in nucleic acid sequence, structure and NMR frequencies, and in efficient chemical depiction, Ph.D. Thesis, Syracuse University, Syracuse, NY.

30. Darlix, J. L., Lapadat-Tapolsky, M., de Rocquigny, H., and Roques, B. P. (1995) First glimpses at structure-function relationships of the nucleocapsid protein of retroviruses, *J. Mol. Biol. 254*, 523−537.
31. Paoletti, A. C. (2004) Affinity of the HIV-1 nucleocapsid protein for structural motifs in the genomic RNA packaging domain, in chemistry, Ph.D. Dissertation, Syracuse University, Syracuse, NY.
32. Kratz, A., and Lewandrowski, K. B. (1998) Case records of the Massachusetts General Hospital. Weekly clinicopathological exercises. Normal reference laboratory values, *N. Engl. J. Med. 339*, 1063−1072.
33. Fisher, R. J., Rein, A., Fivash, M., Urbaneja, M. A., Casas-Finet, J. R., Medaglia, M., and Henderson, L. E. (1998) Sequence-specific binding of human immunodeficiency virus type 1 nucleocapsid protein to short oligonucleotides, *J. Virol. 72*, 1902−1909.
34. Vuilleumier, C., Bombarda, E., Morellet, N., Gerard, D., Roques, B. P., and Mely, Y. (1999) Nucleic acid sequence discrimination by the HIV-1 nucleocapsid protein NCp7: A fluorescence study, *Biochemistry 38*, 16816−16825.
35. Winkler, W. C., and Breaker, R. R. (2005) Regulation of bacterial gene expression by riboswitches, *Annu. Rev. Microbiol. 59*, 487−517.
36. Johansson, J., Mandin, P., Renzoni, A., Chiaruttini, C., Springer, M., and Cossart, P. (2002) An RNA thermosensor controls expression of virulence genes in *Listeria monocytogenes*, *Cell 110*, 551−561.
37. Galagan, J. E., Calvo, S. E., Cuomo, C., Ma, L. J., Wortman, J. R., Batzoglou, S., Lee, S. I., Basturkmen, M., Spevak, C. C., Clutterbuck, J., Kapitonov, V., Jurka, J., Scazzocchio, C., Farman, M., Butler, J., Purcell, S., Harris, S., Braus, G. H., Draht, O., Busch, S., D'Enfert, C., Bouchier, C., Goldman, G. H., Bell-Pedersen, D., Griffiths-Jones, S., Doonan, J. H., Yu, J., Vienken, K., Pain, A., Freitag, M., Selker, E. U., Archer, D. B., Penalva, M. A., Oakley, B. R., Momany, M., Tanaka, T., Kumagai, T., Asai, K., Machida, M., Nierman, W. C., Denning, D. W., Caddick, M., Hynes, M., Paoletti, M., Fischer, R., Miller, B., Dyer, P., Sachs, M. S., Osmani, S. A., and Birren, B. W. (2005) Sequencing of *Aspergillus nidulans* and comparative analysis with *A. fumigatus* and *A. oryzae*, *Nature 438*, 1105−1115.
38. Nudler, E., and Mironov, A. S. (2004) The riboswitch control of bacterial metabolism, *Trends Biochem. Sci. 29*, 11−17.
39. Paillart, J. C., Skripkin, E., Ehresmann, B., Ehresmann, C., and Marquet, R. (1996) A loop-loop "kissing" complex is the essential part of the dimer linkage of genomic HIV-1 RNA, *Proc. Natl. Acad. Sci. U.S.A. 93*, 5572−5577.
40. Laughrea, M., and Jette, L. (1996) Kissing-loop model of HIV-1 genome dimerization: HIV-1 RNAs can assume alternative dimeric forms, and all sequences upstream or downstream of hairpin 248−271 are dispensable for dimer formation, *Biochemistry 35*, 1589−1598.
41. Mujeeb, A., Clever, J. L., Billeci, T. M., James, T. L., and Parslow, T. G. (1998) Structure of the dimer initiation complex of HIV-1 genomic RNA, *Nat. Struct. Biol. 5*, 432−436.
42. Abbink, T. E., Ooms, M., Haasnoot, P. C., and Berkhout, B. (2005) The HIV-1 leader RNA conformational switch regulates RNA dimerization but does not regulate mRNA translation, *Biochemistry 44*, 9058−9066.
43. Huthoff, H., and Berkhout, B. (2002) Multiple secondary structure rearrangements during HIV-1 RNA dimerization, *Biochemistry 41*, 10439−10445.
44. Eichman, B. F., Mooers, B. H., Alberti, M., Hearst, J. E., and Ho, P. S. (2001) The crystal structures of psoralen cross-linked DNAs: Drug-dependent formation of Holliday junctions, *J. Mol. Biol. 308*, 15−26.
45. Ho, P. S., and Eichman, B. F. (2001) The crystal structures of DNA Holliday junctions, *Curr. Opin. Struct. Biol. 11*, 302−308.
46. Doudna, J. A., and Cech, T. R. (1995) Self-assembly of a group I intron active site from its component tertiary structural domains, *RNA 1*, 36−45.
47. Cech, T. R., Herschlag, D., Piccirilli, J. A., and Pyle, A. M. (1992) RNA catalysis by a group I ribozyme. Developing a model for transition state stabilization, *J. Biol. Chem. 267*, 17479−17482.
48. Winkler, W. C., Nahvi, A., Roth, A., Collins, J. A., and Breaker, R. R. (2004) Control of gene expression by a natural metabolite-responsive ribozyme, *Nature 428*, 281−286.
49. Noller, H. F., Kop, J., Wheaton, V., Brosius, J., Gutell, R. R., Kopylov, A. M., Dohme, F., Herr, W., Stahl, D. A., Gupta, R., and Waese, C. R. (1981) Secondary structure model for 23S ribosomal RNA, *Nucleic Acids Res. 9*, 6167−6189.
50. Woodson, S. A., and Leontis, N. B. (1998) Structure and dynamics of ribosomal RNA, *Curr. Opin. Struct. Biol. 8*, 294−300.
51. Gosser, Y., Hermann, T., Majumdar, A., Hu, W., Frederick, R., Jiang, F., Xu, W., and Patel, D. J. (2001) Peptide-triggered conformational switch in HIV-1 RRE RNA complexes, *Nat. Struct. Biol. 8*, 146−150.
52. Sekella, P. T., Rueda, D., and Walter, N. G. (2002) A biosensor for theophylline based on fluorescence detection of ligand-induced hammerhead ribozyme cleavage, *RNA 8*, 1242−1252.
53. Soukup, G. A., and Breaker, R. R. (1999) Design of allosteric hammerhead ribozymes activated by ligand-induced structure stabilization, *Struct. Folding Des. 7*, 783−791.
54. Hartig, J. S., and Famulok, M. (2002) Reporter ribozymes for real-time analysis of domain-specific interactions in biomolecules: HIV-1 reverse transcriptase and the primer-template complex, *Angew. Chem., Int. Ed. 41*, 4263−4266.
55. Nutiu, R., and Li, Y. (2005) Aptamers with fluorescence-signaling properties, *Methods 37*, 16−25.
56. Heyduk, E., and Heyduk, T. (2005) Nucleic acid-based fluorescence sensors for detecting proteins, *Anal. Chem. 77*, 1147−1156.
57. Marshall, K. A., and Ellington, A. D. (1999) Training ribozymes to switch, *Nat. Struct. Biol. 6*, 992−994.
58. Jayasena, S. D. (1999) Aptamers: An emerging class of molecules that rival antibodies in diagnostics, *Clin. Chem. 45*, 1628−1650.
59. Hamaguchi, N., Ellington, A., and Stanton, M. (2001) Aptamer beacons for the direct detection of proteins, *Anal. Biochem. 294*, 126−131.
60. Cavaluzzi, M. J., and Borer, P. N. (2004) Revised UV extinction coefficients for nucleoside-5′-monophosphates and unpaired DNA and RNA, *Nucleic Acids Res. 32*, e13 01−09.
61. Shubsda, M. F., Kirk, C. A., Goodisman, J., and Dabrowiak, J. C. (2000) Binding of human immunodeficiency virus type 1 nucleocapsid protein to psi-RNA-SL3, *Biophys. Chem. 87*, 149−165.
62. Tummino, P. J., Scholten, J. D., Harvey, P. J., Holler, T. P., Maloney, L., Gogliotti, R., Domagala, J., and Hupe, D. (1996) The in vitro ejection of zinc from human immunodeficiency virus (HIV) type 1 nucleocapsid protein by disulfide benzamides with cellular anti- HIV activity, *Proc. Natl. Acad. Sci. U.S.A. 93*, 969−973.
63. Cornille, F., Mely, Y., Ficheux, D., Savignol, I., Gerard, D., Darlix, J. L., Fournie-Zaluski, M. C., and Roques, B. P. (1990) Solid phase synthesis of the retroviral nucleocapsid protein NCp10 of Moloney murine leukaemia virus and related "zinc-fingers" in free SH forms. Influence of zinc chelation on structural and biochemical properties, *Int. J. Pept. Protein Res. 36*, 551−558.
64. Summers, M. F., Henderson, L. E., Chance, M. R., Bess, J. W., South, T. L., Blake, P. R., Sagi, I., Perez-Alvarado, G., Sowder, R. C. I., Hare, D. R., and Arthur, L. O. (1992) Nucleocapsid zinc fingers detected in retroviruses: EXAFS studies of intact viruses and the solution-state structure of the nucleocapsid protein from HIV-1, *Protein Sci. 1*, 563−574.
65. Morellet, N., Demene, H., Teilleux, V., Huynh-Dinh, T., de Rocquigny, H., Fournie-Zaluski, M. C., and Roques, B. P. (1998) Structure of the complex between the HIV-1 nucleocapsid protein NCp7 and the single-stranded pentanucleotide d(ACGCC), *J. Mol. Biol. 283*, 419−434.
66. Mely, Y., Piemont, E., Sorinas-Jimeno, M., de Rocquigny, H., Jullian, N., Morellet, N., Roques, B. P., and Gerard, D. (1993) Structural and dynamic characterization of the aromatic amino acids of the human immunodeficiency virus type I nucleocapsid protein zinc fingers and their involvement in heterologous tRNA-(Phe) binding: A steady-state and time-resolved fluorescence study, *Biophys. J. 65*, 1513−1522.
67. Kerwood, D. J., Cavaluzzi, M. J., and Borer, P. N. (2001) Structure of SL4 RNA from the HIV-1 Packaging Signal, *Biochemistry 40*, 14518−14529.
68. Urbaneja, M. A., Kane, B. P., Johnson, D. G., Gorelick, R. J., Henderson, L. E., and Casas-Finet, J. R. (1999) Binding properties of the human immunodeficiency virus type 1 nucleocapsid protein p7 to a model RNA: Elucidation of the structural determinants for function, *J. Mol. Biol. 287*, 59−75.
69. Amarasinghe, G. K., Zhou, J., Miskimon, M., Chancellor, K. J., McDonald, J. A., Matthews, A. G., Miller, R. R., Rouse, M. D., and Summers, M. F. (2001) Stem-loop SL4 of the HIV-1 ψ RNA packaging signal exhibits weak affinity for the nucleocapsid protein. Structural studies and implications for genome recognition, *J. Mol. Biol. 314*, 961−970.

70. Lawrence, D. C., Stover, C. C., Noznitsky, J., Wu, Z., and Summers, M. F. (2003) Structure of the intact stem and bulge of HIV-1 ψ-RNA stem-loop SL1, *J. Mol. Biol. 326*, 529−542.
71. Fisher, R. J., Fivash, M. J., Stephen, A. G., Hagan, N. A., Shenoy, S. R., Medaglia, M. V., Smith, L. R., Worthy, K. M., Simpson, J. T., Shoemaker, R., McNitt, K. L., Johnson, D. G., Hixson, C. V., Gorelick, R. J., Fabris, D., Henderson, L. E., and Rein, A. (2006) Complex interactions of HIV-1 nucleocapsid protein with oligonucleotides, *Nucleic Acids Res. 34*, 472−484.
72. Tyagi, S., and Kramer, F. R. (1996) Molecular beacons: Probes that fluoresce upon hybridization, *Nat. Biotechnol. 14*, 303−308.
73. Vet, J. A., Majithia, A. R., Marras, S. A., Tyagi, S., Dube, S., Poiesz, B. J., and Kramer, F. R. (1999) Multiplex detection of four pathogenic retroviruses using molecular beacons, *Proc. Natl. Acad. Sci. U.S.A. 96*, 6394−6399.
74. Solinas, A., Brown, L. J., McKeen, C., Mellor, J. M., Nicol, J., Thelwell, N., and Brown, T. (2001) Duplex Scorpion primers in SNP analysis and FRET applications, *Nucleic Acids Res. 29*, e96.
75. Thelwell, N., Millington, S., Solinas, A., Booth, J., and Brown, T. (2000) Mode of action and application of Scorpion primers to mutation detection, *Nucleic Acids Res. 28*, 3752−3761.
76. Rupcich, N., Chiuman, W., Nutiu, R., Mei, S., Flora, K. K., Li, Y., and Brennan, J. D. (2006) Quenching of fluorophore-labeled DNA oligonucleotides by divalent metal ions: Implications for selection, design, and applications of signaling aptamers and signaling deoxyribozymes, *J. Am. Chem. Soc. 128*, 780−790.
77. Anonymous (2006) Black Hole Quenchers. http://www.glenres-.com/.
78. Mathews, D. H., Zuker, M., and Turner, D. H. (2006) *RNAstructure*, version 4.4, University of Rochester, Rochester, NY.
79. Zuker, M. (2006) http://www.bioinfo.rpi.edu/applications/mfold/.
80. Mathews, D. H., Disney, M. D., Childs, J. L., Schroeder, S. J., Zuker, M., and Turner, D. H. (2004) Incorporating chemical modification constraints into a dynamic programming algorithm for prediction of RNA secondary structure, *Proc. Natl. Acad. Sci. U.S.A. 101*, 7287−7292.
81. Mathews, D. H., Sabina, J., Zuker, M., and Turner, D. H. (1999) Expanded sequence dependence of thermodynamic parameters improves prediction of RNA secondary structure, *J. Mol. Biol. 288*, 911−940.
82. SantaLucia, J. (1998) A unified view of polymer, dumbbell, and oligonucleotide DNA nearest-neighbor thermodynamics, *Proc. Natl. Acad. Sci. U.S.A. 95*, 1460−1465.
83. SantaLucia, J., Jr., and Hicks, D. (2004) The thermodynamics of DNA structural motifs, *Annu. Rev. Biophys. Biomol. Struct. 33*, 415−440.
84. Sugimoto, N., Nakano, S., Katoh, M., Matsumura, A., Nakamuta, H., Ohmichi, T., Yoneyama, M., and Sasaki, M. (1995) Thermodynamic parameters to predict stability of RNA/DNA hybrid duplexes, *Biochemistry 34*, 11211−11216.
85. Serra, M. J., and Turner, D. H. (1995) Predicting thermodynamic properties of RNA, *Methods Enzymol. 259*, 242−261.

BI700031J